Published in IET Optoelectronics
Received on 9th September 2013
Revised on 20th January 2014
Accepted on 17th February 2014
doi: 10.1049/iet-opt.2013.0106

ISSN 1751-8768

13.625 Gb/s real-time dual-band adaptive optical orthogonal frequency division multiplexing transmissions over 25 km standard single-mode fibre intensity modulation and direct detection systems utilising strongly saturated reflective semiconductor optical amplifier intensity modulators

Qianwu Zhang[1,2], Emilio Hugues-Salas[1], Roger P. Giddings[1], Junjie Zhang[1,2], Min Wang[2], Jianming Tang[1]

[1]*School of Electronic Engineering, Bangor University, Bangor LL571UT, UK*
[2]*Key Laboratory of Specialty Fiber Optics and Optical Access Networks, Shanghai University, Shanghai 200072, People's Republic of China*
E-mail: zhangqianwu@shu.edu.cn

Abstract: Record-high 13.625 Gb/s real-time end-to-end dual-band optical orthogonal frequency division multiplexing (OFDM) transmissions are experimentally demonstrated over intensity modulation and direct detection-based 25 km standard single-mode fibres utilising 1.125 GHz reflective semiconductor optical amplifier (RSOA) intensity modulators. The 7.375 Gb/s OFDM baseband (0–2 GHz) and 6.25 Gb/s OFDM passband (4.125–8.125 GHz) are adaptively modulated independently and sampled at 4 GS/s. Experimental results show that strongly saturated RSOAs can intensity-modulate adaptive bit- and power-loaded radio frequency (RF) OFDM signals having bandwidths approximately eight times higher than the 3 dB small-signal modulation bandwidths of the RSOAs.

1 Introduction

To satisfy the unprecedented and accelerating increase of end-users' bandwidth requirements [1], optical orthogonal frequency division multiplexing (OOFDM) is regarded as a promising 'future-proof' candidate technology for high-speed passive optical networks (PONs) beyond time and wavelength division multiplexed next generation PONs (NG-PON2), as OOFDM offers high transmission capacity, huge low-cost potential, frequency and time domain dynamic bandwidth allocations, excellent digital signal processing (DSP)-enabled system/network adaptability, as well as good compatibility with conventional time division multiplexing (TDM) PONs [2, 3]. In addition to the aforementioned salient features, centrally controlled universal transceivers are also achievable if use is made of reflective intensity modulators (IMs) in optical network units (ONUs) of OOFDM PONs. To achieve reflective intensity modulation-based cost-effective ONUs, the following reflective IMs may be utilised, which include, for example, reflective semiconductor optical amplifiers (RSOAs) [4], reflective electro-absorption modulators [5–7] and reflective Fabry–Perot lasers [8, 9].

As RSOA-IMs have the advantages including colourlessness, compactness, low power dissipation, large-scale monolithic integration capability and simultaneous functionalities of signal modulation and amplification [10–15], over the past several years, extensive experimental investigations of the performance of RSOA-IM-based OOFDM PONs have been reported using offline DSP, leading to the achievement of 13 Gb/s OOFDM transmissions over 20 km standard single-mode fibres (SSMFs) in wavelength division multiplexing (WDM) OOFDM PONs [16, 17].

Making use of a 1.125 GHz RSOA-IM, we have demonstrated experimentally 7.5 Gb/s real-time end-to-end 16-quadrature amplitude modulation (QAM)-encoded single-band OOFDM (SB-OOFDM) transmissions over 25 km SSMF systems incorporating intensity modulation and direct detection (IMDD) [18, 19]. Compared with SB-OOFDM, multi-band OOFDM (MB-OOFDM) significantly relaxes the requirements of both key component bandwidths and the requisite DSP complexity [20–22]. Most importantly, together with its inherent DSP-rich nature, MB-OOFDM also has unique advantages listed below:

- DSP-controlled intelligence of per-user system/network parameter awareness and automatic performance optimisation. Such function significantly improves the signal transmission capacity, system flexibility, performance robustness and system/network cost-effectiveness.

• Inherent integration of the conventional transceiver functionalities with dynamically configurable channel add/drop networking functionality, thus bringing networking functions to end-users but without adding extra cost to transceivers.
• Provision of DSP-based elastic networking functions. This function can enable network providers to dynamically offer dedicated channels with required performances to end-users without considerably altering network's fibre connections and affecting services provided to other end-users sharing the same networks.

Four-band adaptive OOFDM transmissions of 10 GHz Mach–Zehnder modulator-based 40 Gb/s downstream and 2.5 GHz directly modulated laser-based 10 Gb/s upstream have been experimentally demonstrated using the off-line DSP technique [23]. Making use of real-time field programmable gate arrays (FPGAs), in this paper, we report, for the first time, record-high 13.625 Gb/s real-time end-to-end dual-band adaptive OOFDM transmissions over 25 km SSMF IMDD systems utilising 1.125 GHz RSOA-IMs and 4 GS/s digital-to-analogue converters (DACs)/analogue-to-digital converters (ADCs). More importantly, our experiments also show that, without considerable passband (PB) performance degradation, strongly saturated RSOA-IMs can intensity-modulate adaptive bit-/power-loaded RF OFDM signals having bandwidths approximately eight times higher than the 3 dB small-signal modulation bandwidths of the RSOAs.

Table 1 Transceiver and system parameters

Parameters	Values	Units
Inverse fast Fourier transform (IFFT)/fast Fourier transform (FFT) points per sub-band	32	
data-carrying subcarriers per sub-band	15	
subcarrier frequency spacing	$N \times 125$	MHz
adaptive modulation formats on all subcarriers	16-QAM, 32-QAM, 64-QAM or 128-QAM	
DAC and ADC sample rates	4	GS/s
DAC and ADC resolutions	8	bits
OFDM symbol rate	100	MHz
samples per symbol (IFFT)	32 samples (8 ns)	
cyclic prefix	8 samples (2 ns)	
total samples per symbol	40 samples (10 ns)	
error count period	88 500 symbols	
RSOA small-signal modulation bandwidth	1.125	GHz
RSOA operating temperature	13.5	°C
RSOA bias current	80	mA
RSOA driving voltage	2.5	V_{pp}
Continue wave (CW) optical power injected into the RSOA	4.56	dBm
launched optical power	10.4	dBm
Positive intrinsic negative photodiode (PIN) detector bandwidth	12	GHz
PIN detector sensitivity[a]	– 19	dBm
optical fibre length	25	km
optical fibre type	SSMF	

[a]Corresponding to 10 Gb/s non-return-to-zero data at a BER of 1.0×10^{-9}.

2 Real-time dual-band OOFDM system setup using a RSOA-IM

The RSOA-IM-based real-time end-to-end dual-band OOFDM IMDD transmission system is shown in Fig. 1, where key FPGA-based OFDM DSP functions and transceiver architectures can be found in [24, 25], and the corresponding key transceiver and system parameters adopted in the paper are given in Table 1. In addition, detailed FPGA-based DSPs for real-time OFDM modulation/demodulation have been reported in [26]. To simultaneously generate two separate OFDM sub-band signals, independent digital and RF electronics are employed in each sub-band transmitter [22]: one electrical

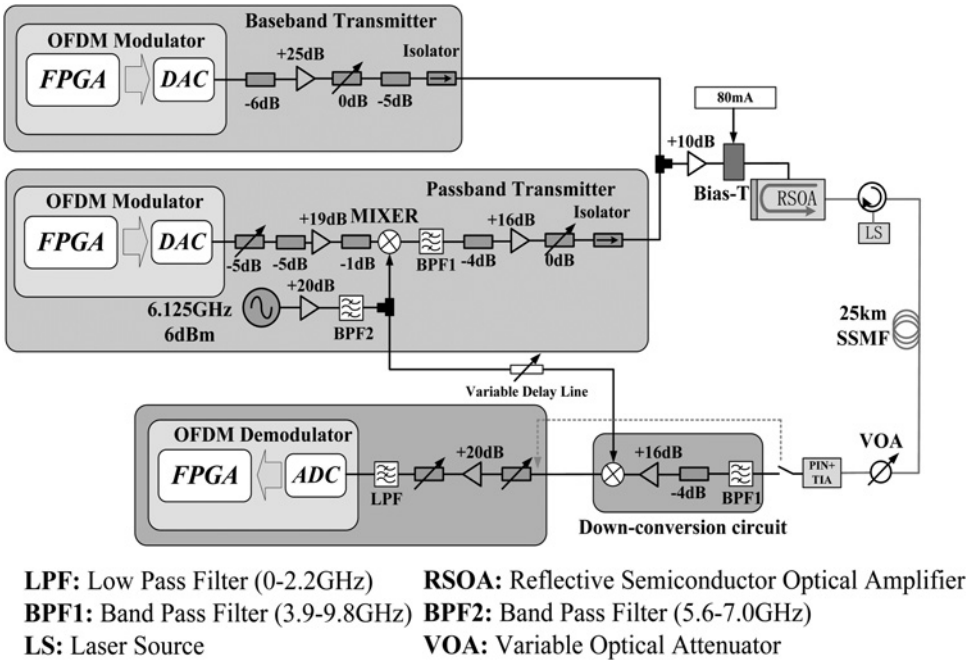

Fig. 1 *Experimental system setup of the RSOA-IM-based 13.625 Gb/s real-time end-to-end dual-band OOFDM system*

doi: 10.1049/iet-opt.2013.0106

sub-band, referred to as the baseband (BB), occupies a spectral region from 0 to 2 GHz, while the second electrical sub-band, known as the PB, is generated by amplitude-modulating a 6.125 GHz RF carrier with another 0–2 GHz OFDM BB signal. This produces the double sideband PB occupying a spectral region from 4.125 to 8.125 GHz. A single receiver is employed to receive either sub-band with the inclusion of an RF down-conversion stage for the PB.

As shown in Fig. 1, at the transmitter side, the real-valued BB signal emerging from the corresponding 4 GS/s, 8 bit DAC is first amplified and its power is appropriately adjusted via variable electrical attenuators (VEAs). Simultaneously, the PB signal is processed by first amplifying an OFDM signal from another 4 GS/s, 8 bit DAC, up-converting with a 6.125 GHz RF carrier via a double-balance mixer, then PB-filtering to attenuate unwanted out-of-band signals, and finally passing through a second RF gain stage with a variable signal power controlled by VEAs. Both the relative sub-band power levels and the absolute dual-band power level can therefore be adjusted with a resolution of 1 dB to allow optimum power levels to be determined. The two sub-bands are finally combined in a 6 dB resistive RF coupler.

After passing through an optical circulator with 1.4 dB insertion loss, a 1550 nm CW optical wave supplied by an external cavity laser source is injected, at an optical power of 4.56 dBm, into a polarisation-insensitive RSOA-IM with a 3 dB small-signal modulation bandwidth of 1.125 GHz and a 3-dB input optical saturation power of about -10 dBm. The 8.125 GHz 2.5 V_{pp} electrical analogue dual-band OFDM signal and an 80 mA DC bias current are combined in a 26.5 GHz bias tee and then modulate the CW optical wave in the RSOA-IM operating at a temperature of 13.5°C. The output optical signal is transmitted through a 25 km SSMF.

At the receiver, the optical signal passes through a variable optical attenuator to adjust the received optical power (ROP). A 12 GHz PIN + TIA is employed to convert the received dual-band OOFDM signal into the electrical domain. To recover the PB (BB) signal, the down-conversion circuit shown in Fig. 1 is included (omitted), which first removes the BB and amplifies the filtered PB prior to RF down-conversion with a double-balance mixer. The received BB signal or the down-converted PB signal passes to the receiver block, where the peak-to-peak signal amplitude is manually adjusted according to the ROP by an RF gain amplifier and a set of VEAs. This is followed by an anti-aliasing low pass filter and balun to generate the differential signal required by the 4 GS/s, 8 bit ADC. Finally, the digital signal emerging from the ADC is directed to the receiver's FPGA to proceed with the inverse OFDM DSP processes compared with its transmitter counterpart [20].

The real-time experimental system has the unique capability of performing on-line analysis of individual subcarrier bit error rates (BERs), overall BER of each sub-band and sub-band system frequency responses, based on which adaptive bit and power loading on each individual subcarrier is undertaken manually, according to the signal-to-noise ratio experienced by the subcarrier, to maximise the signal transmission capacity at the forward error correction (FEC) limit of 2.3×10^{-3}. The OOFDM transceiver DSP design identical to that reported in [24] is adopted, which enables the highest possible signal modulation format to be selected from 16-QAM, 32-QAM, 64-QAM and 128-QAM. Clearly, such a design offers an excellent opportunity of rapidly optimising the overall system performance.

Here it is also worth mentioning the following three aspects: (i) for both mixers in the PB transmitter and receiver sides, the local oscillator (LO) signals are derived from the same RF signal source and a variable delay line is employed to correctly align the phase of the receiver's LO with the phase of the received RF carrier. The RF up-conversion and down-conversion circuits have standard configuration complexity and employ off-the-shelf electronics. Therefore, their cost is expected to be low in high volume for cost-sensitive applications. (ii) Owing to the combined effects of fibre chromatic dispersion, RSOA intensity modulation-induced frequency chirp and direct detection in the receiver, the system frequency response has a second peak occurring at approximately 7 GHz. The PB carrier frequency adopted in the paper enables the PB to occupy the peak region of the system frequency response. And (iii) the utilisation of the external cavity laser illustrated in Fig. 1 is to provide a sufficiently large optical power dynamic range to enable us to measure the RSOA gain saturation-related effects. The laser can be replaced by other commercially available lasers such as distributed feedbacks or vertical cavity surface emitting lasers without compromising the system BER performance.

3 Experimental results

Fig. 2*a* shows the normalised frequency response roll-off of each sub-band for the entire RSOA-IM-based IMDD 25 km SSMF system measured from the transmitter IFFT input to the receiver FFT output at 1550 nm. For the PB case, an effective system frequency response is measured before (after) RF up(down)-conversion in the transmitter (receiver). This allows the effect of PB transmission-induced relative

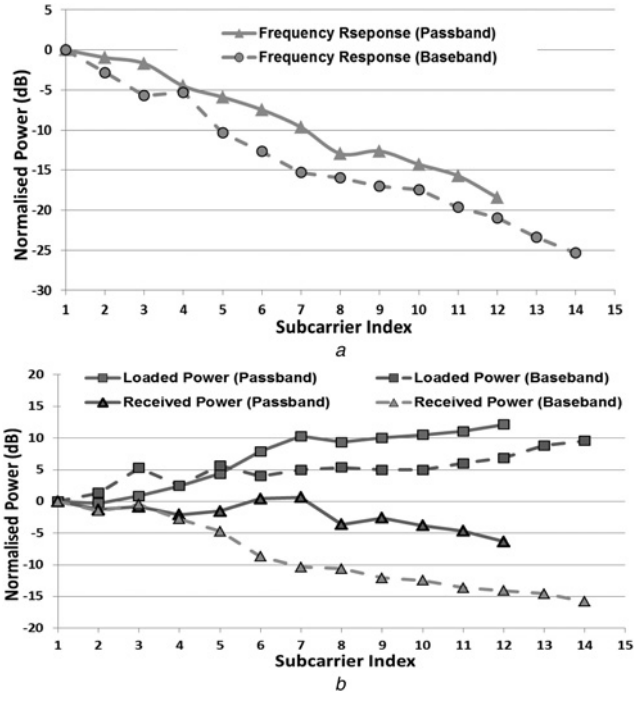

Fig. 2 *Experimental results*

a Normalised system frequency responses for both sub-bands
b Relative loaded/received subcarrier powers for both sub-bands

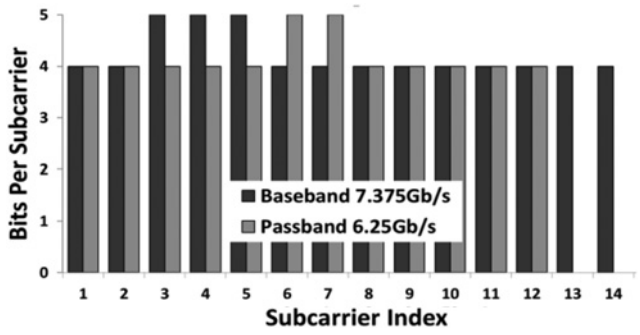

Fig. 3 *Adaptive bit allocation profiles for the RSOA-IM-based dual-band OOFDM system*

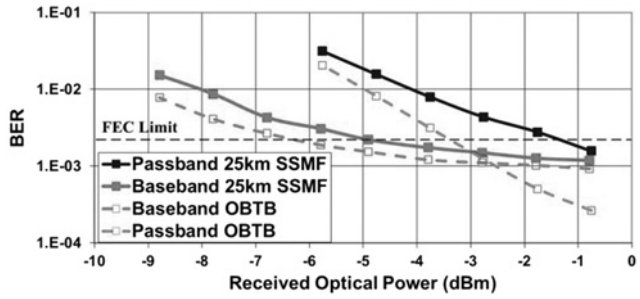

Fig. 4 *Measured BB and PB BER performance for both optical back-to-back and entire 25 km SSMF system*

subcarrier attenuation to be included, but this does not reveal the true system frequency response of the RF and optical channels in the PB region of 4.125–8.125 GHz. In Fig. 2*a* similar frequency response roll-offs of approximately 20 dB are observed for high frequency subcarriers of both sub-bands. Therefore, adaptive bit and power loading has to be adopted at the 15 information-bearing subcarriers of each sub-band to compensate for the observed large frequency response roll-off effect.

The resulting adaptively loaded/received subcarrier power profiles and the corresponding online optimised bit loading profiles are presented in Figs. 2*b* and 3, respectively, for both sub-bands. In Fig. 2*b*, the loaded power of the eighth subcarrier in the PB is slightly lower than those corresponding to the seventh subcarrier and ninth subcarrier of the same sub-band may be resulted from limited cyclic prefix duration-induced imperfect subcarrier orthogonality, which generates unwanted subcarrier intermixing noises unevenly distributed among various subcarriers. Considering Fig. 3 and the above-mentioned transceiver parameters, it is easy to calculate that the achieved BB signal bit rate is 7.375 Gb/s and the achieved PB signal bit rate is 6.25 Gb/s, thus giving rise to an aggregated signal transmission capacity of 13.625 Gb/s, of which 10.9 Gb/s can be utilised to convey user data, because a 25% cyclic prefix is adopted which can, however, be reduced when the present real-time OOFDM transceiver DSP design is modified. It should also be noted in Fig. 3 that the inter-sub-band intermixing effect and the limited FPGA and DAC power dynamic range-induced imperfect compensation of the frequency response roll-off leads to the completely dropping of the last subcarrier in the BB and the last three subcarriers in the PB.

For the optical back-to-back and entire 25 km IMDD SSMF transmission systems, Fig. 4 presents measured total BER performances of the 7.375 Gb/s BB and 6.25 Gb/s PB as a function of ROP. Fig. 5 illustrates representative subcarrier constellations measured for each sub-band prior to equalisation. In this figure, three constellations are shown for each sub-band: one for the lowest frequency subcarrier, one for the highest frequency subcarrier and one for the subcarrier having a frequency in the middle. It can be seen in Fig. 4 that, in comparison with the PB, the relatively flat BER developing curve for the BB at high ROPs is due to the fact that unwanted inter- and intra-sub-band intermixing frequency products generated on square-law photon detection in the receiver are predominantly located in the BB spectral region. Comparing the BB with the PB, the observed difference in ROP at the adopted FEC limit of 2.3×10^{-3} for the back-to-back cases is a direct result of the residual frequency response roll-off effect caused by the imperfect roll-off compensation mentioned previously. Moreover, compared with the BB, the larger power penalty for the PB is mainly contributed by the broad PB bandwidth ($\sim$16 GHz)-enhanced chromatic dispersion effect.

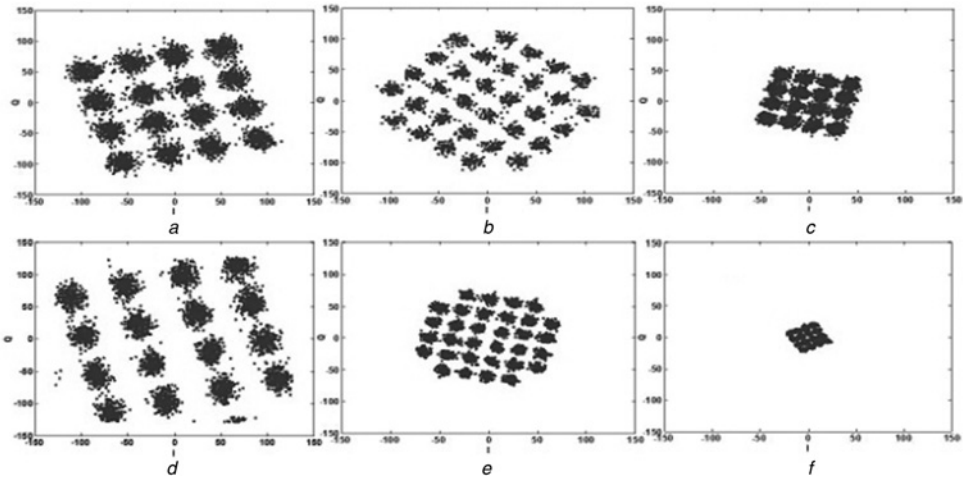

Fig. 5 *Received constellations of representative subcarriers before channel equalisation after 25 km SSMF transmission (PB: passband and BB: baseband)*

a PB 1st SC *c* PB 12th SC *e* BB 5nd SC
b PB 7th SC *d* BB 1st SC *f* BB 14nd SC

doi: 10.1049/iet-opt.2013.0106

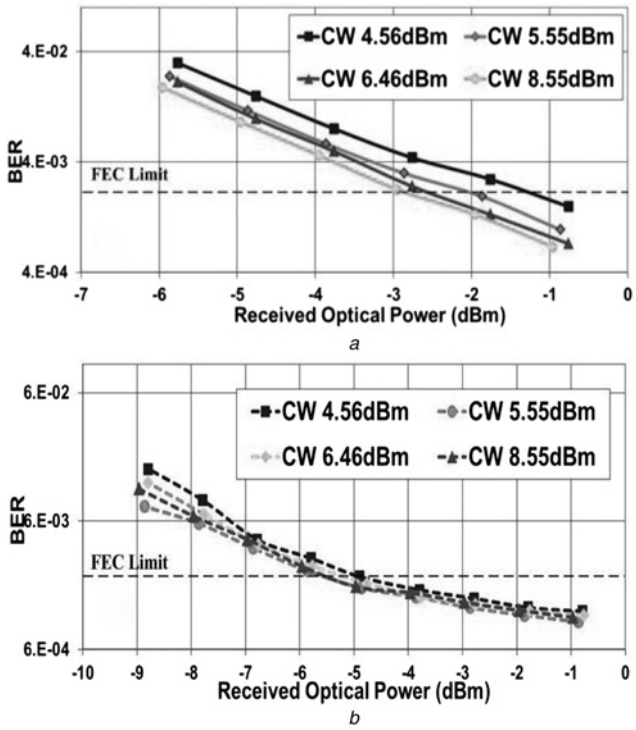

Fig. 6 *BER performances under different injected CW optical powers*

a PB
b BB

It is also very interesting to note in Fig. 4 that, for ROPs larger than approximately −2 dBm, very similar BERs for both sub-bands occur, indicating that strongly saturated RSOA-IMs can support successful transmissions of adaptively modulated OFDM signals having bandwidths far beyond their 3 dB small-signal modulation bandwidths. This statement can also be verified in Fig. 3, where identical signal modulation formats are taken on the majority of subcarriers for each sub-band. To further explore the above statement, the injected CW optical power-dependent BER against ROP performances are shown in Figs. 6*a* and *b* for the PB and BB, respectively. It can be seen in Fig. 6*a* that a 1.4 dB ROP reduction for the PB is achievable when the injected CW optical power is increased from 4.56 to 8.55 dBm, over which the ROP for the BB, however, remains almost the same, as shown in Fig. 6*b*. The physical mechanism underpinning such behaviours is that a highly saturated RSOA-IM results in a decreased carrier lifetime [10], which lifts up the RSOA-IM modulation response in the high-frequency region, whereas the modulation response in the low-frequency region remains almost unchanged.

4 Conclusions

About 13.625 Gb/s over 25 km SSMF real-time end-to-end dual-band adaptive OOFDM IMDD transmissions have been experimentally demonstrated utilising 1.125 GHz RSOA-IMs and 4 GS/s DACs/ADCs. For strongly saturated RSOA-IMs, the bandwidths of adaptively modulated OFDM signals can be well above the typical small-signal RSOA modulation bandwidth. This can significantly relax the requirements of RSOA modulation bandwidths for achieving a specific transmission capacity. The proof-of-principle experimental demonstrations reported in this paper can be extended to include more sub-bands to further improve the aggregated system transmission capacity.

5 Acknowledgments

This work was supported by the PIANO+ under the European Commission's ERA-NET Plus Scheme within the project OCEAN under grant agreement 620029 and in part by the National Natural Science Foundation of China (61132004).

6 References

1 Vetter, P.: 'Next generation optical access technologies'. Proc. European Conf. Optical Communication (ECOC), Amsterdam, 2012, Paper Tu. 3. G. 1
2 Jin, X.Q., Tang, J.M.: 'Experimental investigations of wavelength spacing and colorlessness of RSOA-based ONUs in real-time optical OFDMA PONs', *J. Lightwave Technol.*, 2012, **30**, (16), pp. 2603–2609
3 Qian, D., Cvijetic, N., Hu, J., Wang, T.: 'Optical OFDM transmission in metro/access networks'. Proc. Optical Fiber Communication Conf. (OFC), San Diego, CA, USA, 2009, Paper OMV1
4 Yeh, C.H., Chow, C.W., Chen, H.Y., Wu, Y.F.: '10-Gbps OFDM upstream rate by using RSOA-ONU with seeding-light for 75 km long-reach PON access'. Proc. Optical Fiber Communication Conf. (OFC), Los Angeles, CA, USA, 2012, Paper JTh2A
5 Ossieur, P., Antony, C., Clarke, A.M., *et al.*: 'A 135-km 8192-split carrier distributed DWDM-TDMA PON with 2 × 32 10 Gb/s capacity', *J. Lightwave Technol.*, 2011, **29**, (4), pp. 463–474
6 Borghesani, A.: 'Reflective based active semiconductor components for next generation optical access networks'. Proc. European Conf. Optical Communication (ECOC), Torino, 2010, Paper Mo.1.B.1
7 Lin, S.C., Lee, S.L., Liu, C.K., *et al.*: 'Design and demonstration of REAM-based WDM-PONs with remote amplification and channel fault monitoring', *J. Opt. Commun. Netw.*, 2012, **4**, (4), pp. 336–343
8 Xu, Z., Yeo, Y., Cheng, X., Kurniawan, E.: '20-Gb/s injection locked FP-LD in a wavelength-division multiplexing OFDM-PON'. Proc. Optical Fiber Communication Conf. (OFC), Los Angeles, CA, USA, 2012, Paper OW4B.3
9 Lee, C.H.: 'WDM-PON overview'. Proc. European Conf. Optical Communication (ECOC), Vienna, 2009, Paper 5.7.1
10 Wei, J.L., Hamié, A., Gidding, R.P., *et al.*: 'Adaptively modulated optical OFDM modems utilizing RSOAs as intensity modulators in IMDD SMF transmission systems', *Opt. Express*, 2010, **18**, (8), pp. 8556–8573
11 Omella, M., Polo, V., Lazaro, J., Schrenk, B., Prat, J.: '10 Gb/s RSOA transmission by direct duobinary modulation'. Proc. European Conf. Optical Communication (ECOC), Brussels, 2008, Paper Tu.3.E.4
12 Lee, W., Park, M.H., Cho, S.H., *et al.*: 'Bidirectional WDM-PON based on gain saturated reflective semiconductor optical amplifiers', *IEEE Photonics Technol. Lett.*, 2005, **17**, (11), pp. 2460–2462
13 Cho, K.Y., Takushima, Y., Chung, Y.C.: '10-Gb/s operation of RSOA for WDM PON', *IEEE Photonics Technol. Lett.*, 2008, **20**, (18), pp. 1533–1535
14 Yeh, C.H., Chow, C.W., Wang, C.H., Shih, F.Y., Chien, H.C., Chi, S.: 'A self-protected colorless WDM-PON with 2.5 Gb/s upstream signal based on RSOA', *Opt. Express*, 2008, **16**, (16), pp. 12296–12301
15 Omella, M., Papagiannakis, I., Schrenk, B., *et al.*: '10 Gb/s full-duplex bidirectional transmission with RSOA-based ONU using detuned optical filtering and decision feedback equalization', *Opt. Express*, 2009, **17**, (7), pp. 5008–5013
16 Duong, T., Genay, N., Chanclou, P., Charbonnier, B., Pizzinat, A., Brenot, R.: 'Experimental demonstration of 10 Gbit/s for upstream transmission by remote modulation of 1 GHz RSOA using adaptively modulated optical OFDM for WDM-PON single fiber architecture'. Proc. European Conf. Optical Communication (ECOC), Brussels, 2008, Paper Th.3.F.1
17 Chow, C.W., Yeh, C.H., Wu, Y.F., *et al.*: '13 Gbit/s WDM-OFDM PON using RSOA-based colourless ONU with seeding light source in local exchange', *Electron. Lett.*, 2011, **47**, (22), pp. 1235–1236
18 Giddings, R.P., Hugues-Salas, E., Jin, X.Q., Wei, J.L., Tang, J.M.: 'Experimental demonstration of real-time optical OFDM transmission at 7.5 Gb/s over 25-km SSMF using a 1-GHz RSOA', *Photonics Technol. Lett.*, 2010, **22**, (11), pp. 745–747
19 Giddings, R.P., Hugues-Salas, E., Jin, X.Q., Wei, J.L., Tang, J.M.: 'Colourless real-time optical OFDM end-to-end transmission at 7.5 Gb/s over 25 km SSMF using 1 GHz RSOAs for WDM-PONs'. Proc.

Optical Fiber Communication Conf. (OFC), San Diego, CA, USA, 2010, Paper OMS4
20 Giddings, R.P., Hugues-Salas, E., Tang, J.M.: 'Experimental demonstration of record high 19.125 Gb/s real-time end-to-end dual-band optical OFDM transmission over 25 km SMF in a simple EML-based IMDD system', *Opt. Express*, 2012, **20**, (18), pp. 20666–20679
21 Hugues-Salas, E., Zhang, Q.W., Giddings, R.P., Wang, M., Tang, J.M.: 'Adaptability-enabled record-high and robust capacity versus reach performance of real-time dual-band optical OFDM signals over various OM1/OM2 MMF systems [invited]', *J. Opt. Commun. Netw.*, 2013, **5**, (10), pp. A1–A11
22 Zhang, Q.W., Hugues-Salas, E., Giddings, R.P., Wang, M., Tang, J.M.: 'Experimental demonstrations of record high REAM intensity modulator-enabled 19.25 Gb/s real-time end-to-end dual-band optical OFDM colorless transmissions over 25 km SSMF IMDD systems', *Opt. Express*, 2013, **21**, (7), pp. 9167–9179
23 Yeh, C.H., Chow, C.W., Chen, H.Y., Chen, B.W.: 'Using adaptive four-band OFDM modulation with 40 Gb/s downstream and 10 Gb/s upstream signals for next generation long-reach PON', *Opt. Express*, 2011, **19**, (27), pp. 26150–26160
24 Jin, X.Q., Wei, J.L., Giddings, R.P., Quinlan, T., Walker, S., Tang, J.M.: 'Experimental demonstrations and extensive comparisons of end-to-end real-time optical OFDM transceivers with adaptive bit and/or power loading', *IEEE Photonics J.*, 2011, **3**, (3), pp. 500–511
25 Giddings, R.P., Jin, X.Q., Hugues-Salas, E., Giacoumidis, E., Wei, J.L., Tang, J.M.: 'Experimental demonstration of a record high 11.25 Gb/s real-time optical OFDM transceiver supporting 25 km SMF end-to-end transmission in simple IMDD systems', *Opt. Express*, 2010, **18**, (6), pp. 5541–5555
26 Giddings, R.P.: 'Real-time digital signal processing for optical OFDM-based future optical access networks', *J. Lightwave Technol.*, 2014, **32**, (4), pp. 553–570

doi: 10.1049/iet-opt.2013.0106